PROCEEDINGS, 46th Workshop on Geothermal Reservoir Engineering
Stanford University, Stanford, California, February 15-17, 2021
SGP-TR-218

Temporal-Spatial Evolution of Anisotropic Rock Properties during Hydraulic Fracture Stimulations at the First EGS Collab Testbed

Zongcai Feng[1], Benxin Chi[1], Lianjie Huang[1], Kai Gao[1], Jiaxuan Li[1], Jonathan Ajo-Franklin[2], Pengcheng Fu[3], Timothy J. Kneafsey[4], and The EGS Collab Team[5]

[1]Los Alamos National Laboratory, Los Alamos, NM 87545, USA

[2]Rice University, Houston, TX 77005, USA

[3]Lawrence Livermore National Laboratory, Livermore, CA 94551, USA

[4]Lawrence Berkeley National Laboratory, Berkeley, CA 94720, USA

[5]The EGS Collab Team

zongcai@lanl.gov; ljh@lanl.gov

Keywords: Anisotropic, CASSM, continuous active-source seismic monitoring, EGS Collab, elastic-waveform inversion, enhanced geothermal systems, hydraulic fracture stimulation, seismic monitoring, time-lapse, traveltime tomography

ABSTRACT

The EGS Collab project acquired continuous active-source seismic monitoring (CASSM) data before, during, and after hydraulic stimulations at the first testbed at the depth of 4850 ft at the Sanford Underground Research Facility in Lead, South Dakota, for monitoring fracture creation and evolution. CASSM monitoring used 24 hydrophones, 18 accelerometers, and 17 dipole sources within four fracture-parallel wells and two orthogonal wells. 3D anisotropic traveltime tomography and anisotropic elastic-waveform inversion of the campaign cross-borehole seismic data show that the rock within the stimulation region is a heterogeneous horizontal transverse isotropic medium. We use these inversion results as the initial models and apply 3D anisotropic first-arrival traveltime tomography and 3D anisotropic elastic-waveform inversion to the CASSM data acquired after each stimulation in May, 2018 and December, 2018. We observe the temporal and spatial evolution of seismic velocities and anisotropic parameters caused by hydraulic fracture stimulations, showing the regions of rock alternation caused by hydraulic fracture stimulation.

1. INTRODUCTION

The EGS Collab project, supported by the U.S. Department of Energy Geothermal Technologies Office, is studying permeability enhancement and evolution in crystalline rocks for heat extraction using fracture stimulations (Kneafsey et al., 2020, 2021). The first EGS Collab testbed, Experiment 1, is located at the depth of 4850 ft at the Sanford Underground Research Facility (SURF) in Lead, South Dakota. The purpose of the Experiment 1 is to establish a fracture network that connects an injection well and a production well using hydraulic fracturing. Advanced seismic imaging and inversion methods were used to characterize the rock and monitor the changes of rock properties during stimulation. The methods used include anisotropic traveltime tomography (Gao et al., 2019) and anisotropic elastic-waveform inversion for the campaign cross-borehole seismic data (Gao et al., 2020), and elastic-waveform inversion and least-squares reverse-time migration for the continuous active-source seismic monitoring (CASSM) data (Pan el al., 2019; Chi el al., 2019, 2020).

The CASSM system contains 17 dipole sources, two cemented hydrophone strings with 12 sensors at 1.75 m spacing, and 18 3-C accelerometers deployed in the six monitoring boreholes. The project acquired CASSM data continuously for several months to monitor fractures created by hydraulic stimulations in May and December 2018. In this research, we use the CASSM data to study temporal-

[5]J. Ajo-Franklin, T. Baumgartner, K. Beckers, D. Blankenship, A. Bonneville, L. Boyd, S. Brown, J.A. Burghardt, C. Chai, A. Chakravarty, T. Chen, Y. Chen, B. Chi, K. Condon, P.J. Cook, D. Crandall, P.F. Dobson, T. Doe, C.A. Doughty, D. Elsworth, J. Feldman, Z. Feng, A. Foris, L.P. Frash, Z. Frone, P. Fu, K. Gao, A. Ghassemi, Y. Guglielmi, B. Haimson, A. Hawkins, J. Heise, Chet Hopp, M. Horn, R.N. Horne, J. Horner, M. Hu, H. Huang, L. Huang, K.J. Im, M. Ingraham, E. Jafarov, R.S. Jayne, T.C. Johnson, S.E. Johnson, B. Johnston, S. Karra, K. Kim, D.K. King, T. Kneafsey, H. Knox, J. Knox, D. Kumar, K. Kutun, M. Lee, D. Li, J. Li, K. Li, Z. Li, M. Maceira, P. Mackey, N. Makedonska, C.J. Marone, E. Mattson, M.W. McClure, J. McLennan, T. McLing, C. Medler, R.J. Mellors, E. Metcalfe, J. Miskimins, J. Moore, C.E. Morency, J.P. Morris, T. Myers, S. Nakagawa, G. Neupane, G. Newman, A. Nieto, T. Paronish, R. Pawar, P. Petrov, B. Pietzyk, R. Podgorney, Y. Polsky, J. Pope, S. Porse, J.C. Primo, C. Reimers, B.Q. Roberts, M. Robertson, V. Rodriguez-Tribaldos, W. Roggenthen, J. Rutqvist, D. Rynders, M. Schoenball, P. Schwering, V. Sesetty, C.S. Sherman, A. Singh, M.M. Smith, H. Sone, E.L. Sonnenthal, F.A. Soom, D.P. Sprinkle, S. Sprinkle, C.E. Strickland, J. Su, D. Templeton, J.N. Thomle, C. Ulrich, N. Uzunlar, A. Vachaparampil, C.A. Valladao, W. Vandermeer, G. Vandine, D. Vardiman, V.R. Vermeul, J.L. Wagoner, H.F. Wang, J. Weers, N. Welch, J. White, M.D. White, P. Winterfeld, T. Wood, S. Workman, H. Wu, Y.S. Wu, E.C. Yildirim, Y. Zhang, Y.Q. Zhang, Q. Zhou, M.D. Zoback

spatial evolution of the rock properties during five hydraulic stimulations performed in May, 2018 and two hydraulic stimulations in December, 2018.

Previous research has shown that the host rock at the first EGS Collab testbed for Experiment 1 is anisotropic (Johnson et al., 2019; Gao et al., 2019, 2020). Seismic wave is a superposition of quasi-P (qP) and quasi-S (qS) waves when propagating in an anisotropic medium (Tsvankin, 1996). We firstly perform 3D anisotropic traveltime tomography of the CASSM data using the extrapolated models obtained using 3D anisotropic traveltime tomography and 3D anisotropic elastic-waveform inversion of the campaign cross-borehole seismic data (Gao et al., 2020) as the initial model. We then use 3D anisotropic elastic-waveform inversion of the CASSM data to improve the traveltime tomography result and obtain high-resolution anisotropic elastic parameter models, including qP- and qS-wave velocities along the symmetry axis, Thomsen parameters, and density. We analyze the time-lapse CASSM data to obtain traveltime variations of both qP- and qS-wave arrivals caused by hydraulic fracture stimulations. We finally employ 3D double-difference anisotropic elastic-waveform inversion of the time-lapse CASSM data using the traveltime variations as the misfit function to obtain the temporal-spatial evolution of elastic parameters. Our results show the temporal and spatial evolution of qP- and qS-wave velocities and anisotropic parameters caused by hydraulic fracture stimulations after each stimulation in May, 2018 and in December, 2018. Such regions of rock alternation could be caused by created fractures, opening of existing fractures, injected water, and temperature changes.

2. METHODOLOGY

We use the 3D anisotropic adjoint-state first-arrival traveltime tomography method to invert for a set of best-fit anisotropic models (Gao et al., 2020). The method seeks to match the synthetic first-arrival traveltimes with the observed first-arrival times:

$$(V_{p0}, \epsilon, \delta)^* = \arg\min_{V_{p0},\epsilon,\delta} \left\| T_{\text{obs}} - T_{\text{syn}} \right\|^2, \tag{1}$$

where V_{p0}, ϵ, and δ are the phase velocity of qP wave and Thomsen parameters, respectively. We solve the 3D anisotropic eikonal equation to obtain the first-arrival traveltime associated with the qP-wave mode, and update the medium parameters using the gradients calculated using the adjoint-state eikonal equation (Gao et al., 2020).

We further use 3D anisotropic elastic-waveform inversion to update elastic anisotropic medium parameter model $\mathbf{m}$ by minimizing the observed seismic waveform $\mathbf{d}_{\text{baseline}}$ and the synthetic waveform $\mathbf{u}_{\text{baseline}}$ computed using 3D anisotropic elastic-wave equation (Gao et al., 2020):

$$\mathbf{m} = \arg\min_{\mathbf{m}} \left\| \mathbf{u}_{\text{baseline}} - \mathbf{d}_{\text{baseline}} \right\|^2, \text{ where } \mathbf{m} \text{ is } (V_{p0}, V_{s0}, \rho, \epsilon, \delta, \gamma), \tag{2}$$

where V_{p0} and V_{s0} are the phase velocities of qP and qS waves along the symmetry axis, respectively, ρ is the medium density, and ϵ, δ, and γ are Thomsen parameters. In a horizontal transverse isotropic (HTI) medium, the phase velocities of qP and qS waves depend on the propagation direction θ with respect to the symmetry axis (Berryman, 2008):

$$\begin{aligned}
V_p(\theta)/V_{p0} &\simeq 1 - \frac{\varepsilon}{1+2\varepsilon}\sin^2\theta - \frac{\varepsilon-\delta}{1+2\varepsilon}\frac{2A\sin^2\theta\cos^2\theta}{1-B\cos 2\theta}, \\
V_{sv}(\theta)/V_{sv0} &\simeq 1 + [c_{33}/c_{44}](\varepsilon-\delta)\frac{2A\sin^2\theta\cos^2\theta}{[1-B\cos 2\theta]}, \\
V_{sh}(\theta)/V_{sh0} &\simeq 1 - \frac{\gamma}{1+2\gamma}\sin^2\theta,
\end{aligned} \tag{3}$$

$$\text{with } V_{p0} = \sqrt{c_{11}/\rho} = \sqrt{c_{33}(1+2\epsilon)/\rho},\ V_{sv0} = \sqrt{c_{44}/\rho},\ V_{sh0} = \sqrt{c_{66}/\rho} = \sqrt{c_{44}(1+2\gamma)/\rho},\ A = \frac{c_{33}-c_{44}}{2[(1+\epsilon)c_{33}-c_{44}]} \text{ and } B = \frac{\epsilon c_{33}}{(1+\epsilon)c_{33}-c_{44}},$$

where V_{sv} and V_{sh} are corresponds to the quasi-SV- and quasi-SH-wave modes, respectively, and c_{ij} (i, j=1, 2, … 6) is the stiffness matrix. V_{sv0} is denoted as V_{s0} in the flowing.

After updating model $\mathbf{m}$, we can update its time-lapse difference model $\Delta\mathbf{m}$ by using double-difference elastic waveform inversion (Zhang and Huang, 2013):

$$\Delta\mathbf{m} = \arg\min_{\Delta\mathbf{m}} \left\| (\mathbf{u}_{\text{monitor}} - \mathbf{u}_{\text{baseline}}) - (\mathbf{d}_{\text{monitor}} - \mathbf{d}_{\text{baseline}}) \right\|^2, \text{ where } \Delta\mathbf{m} \text{ is } (\Delta V_{p0}, \Delta V_{s0}, \Delta\rho, \Delta\epsilon, \Delta\delta, \Delta\gamma). \tag{4}$$

However, the convergence of double-difference waveform inversion in the form of equation (2) may be severely impacted by the noise and other amplitude factors in data. To improve inversion convergence, we use the traveltime difference instead of the waveform difference to update the time-lapse model difference (Luo and Schuster, 1991):

$$\Delta\mathbf{m} = \arg\min_{\Delta\mathbf{m}} \left\| \Delta T_{\mathbf{u}}(\mathbf{u}_{monitor}, \mathbf{u}_{baseline}) - \Delta T_{\mathbf{d}}(\mathbf{d}_{monitor}, \mathbf{d}_{baseline}) \right\|^2 , \quad (5)$$

where ΔT is the traveltime difference of two traces obtained using cross correlation, which is more accurate than hand picking.

3. RESULTS OF BASELINE

3.1 CASSM acquisition system

Figure 1a shows the CASSM data acquisition system in Experiment 1: the green and red lines are injection and production wells, respectively, and the black lines are six monitoring wells. The CASSM monitoring involves the repeated activation of the 17 sources at green rectangles and receivers of the permanent 24 hydrophones at blue circles and 18 accelerometers at red triangles.

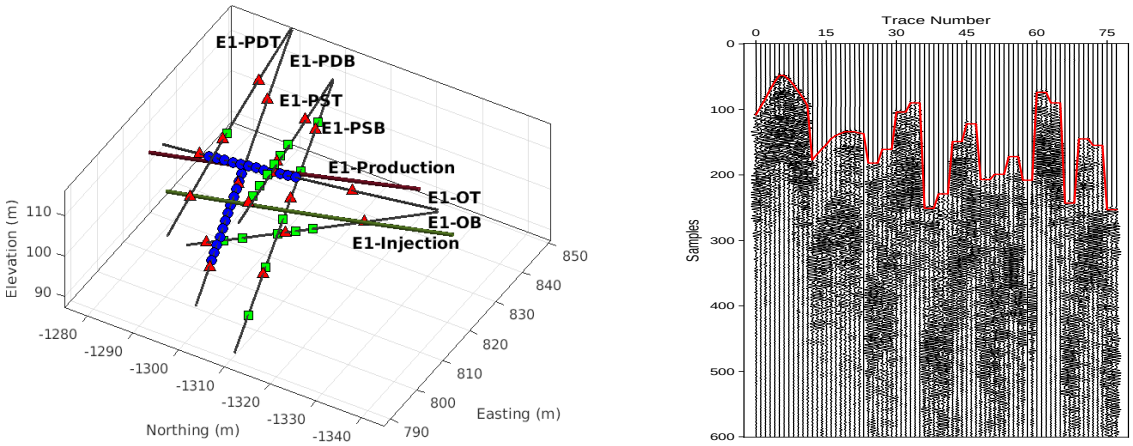

a b

Figure 1: (a) The CASSM data acquisition system at the EGS Collab Experiment 1. The red, green, and black lines represent the injection (E1-Injection), production (E1-Production), and six monitoring wells (E1-OT, E1-OB, E1-PSB, E1-PST, E1-PDB, E1-PDT), respectively. The green rectangles, blue circles, and red triangles indicate 17 CASSM sources, 24 hydrophones, and 18 accelerometers, respectively. (b) One common-shot gather of the CASSM data and the corresponding picked first-arrival traveltimes (Chi el al., 2020).

3.2 Scattering and traveltime analyses of the CASSM data

We use the CASSM data recorded from 05/21/2018 to 05/27/2018 and from 12/20/2018 to 12/23/2018 to perform 3D anisotropic traveltime tomography and 3D anisotropic elastic-waveform inversion, and study the temporal-spatial evaluation of rock properties during the stimulations. Figure 2a and 2d show one source-receiver CASSM dataset that cross the potential fracture in May, 2018 and December, 2018, respectively. The scattering waveform differences in Figure 2b and 2e are caused by the hydraulic stimulations, including created fractures and injected water. We obtain the waveform differences by subtracting the waveforms recorded before the first stimulation in May, 2018 and in December, 2018, respectively.

We compute the time-lapse changes of first-arrival traveltimes using cross correlation, and display the results in Figure 2c and 2f. The red circles in Figure 2c and 2f indicate 5 stimulations and 2 stimulations performed in May, 2018 and in December, 2018, respectively.

These time-lapse changes of traveltimes in the CASSM data can be used to monitor the hydraulic stimulation process. In the first two stimulations in May, 2018, the scattering and the traveltime changes caused by the created fracture and injected water is weak because the size of the created fracture is small. During the last three stimulations, a larger fracture was created to connect the injection and the production wells, leading to very strong scattering and traveltime changes detected in the CASSM data (Chi el al., 2020). We use the time-lapse changes of the CASSM data to invert for the temporal-spatial evolution of rock properties during hydraulic fracture stimulations.

3.3 Initial model and 3D anisotropic traveltime tomography of the baseline CASSM data in May 2018

3D anisotropic traveltime tomography and 3D anisotropic elastic-waveform inversion of the campaign cross-borehole seismic data show that the rock within the stimulation region is a heterogeneous HTI medium (Gao et al., 2019, 2020). We extrapolate those results to construct the initial models for inverting the time-lapse CASSM data. Figure 3a is the initial V_{p0} model within the CASSM data acquisition region obtained from inversion of the campaign cross-borehole seismic data, and Figure 3b shows the initial V_{p0} model for traveltime tomography after extrapolating the V_{p0} model in Figure 3a. We also extrapolate V_{s0}, density, and Thomsen parameters.

We perform 3D anisotropic traveltime tomography of the first-arrival traveltimes of qP-wave events of the CASSM data acquired on May 21, 2018 before hydraulic stimulation. The inverted V_{p0} and Thomsen parameters ϵ and δ models are shown in Figure 4.

3.4 3D anisotropic elastic-waveform inversion of the baseline CASSSM data in May 2018

For 3D anisotropic elastic-waveform inversion, we window out the qP- and the qS-wave direct arrivals in the baseline CASSM data acquired before hydraulic stimulation in May, 2018, and use them to further update the velocity and anisotropic models with the inverted V_{p0} and Thomsen parameters e and d of the traveltime tomography as the initial models. Our 3D anisotropic elastic-waveform inversion also used the extrapolated V_{s0}, density, and Thomsen parameters g as the initial parameter models. We continue to perform 3D anisotropic elastic-waveform inversion of the data, and show the inverted V_{p0}, V_{s0}, and Thomsen parameters e, d, and g models in Figure 5. Our final 3D anisotropic elastic-waveform inversion results further refine the models of 3D anisotropic traveltime tomography.

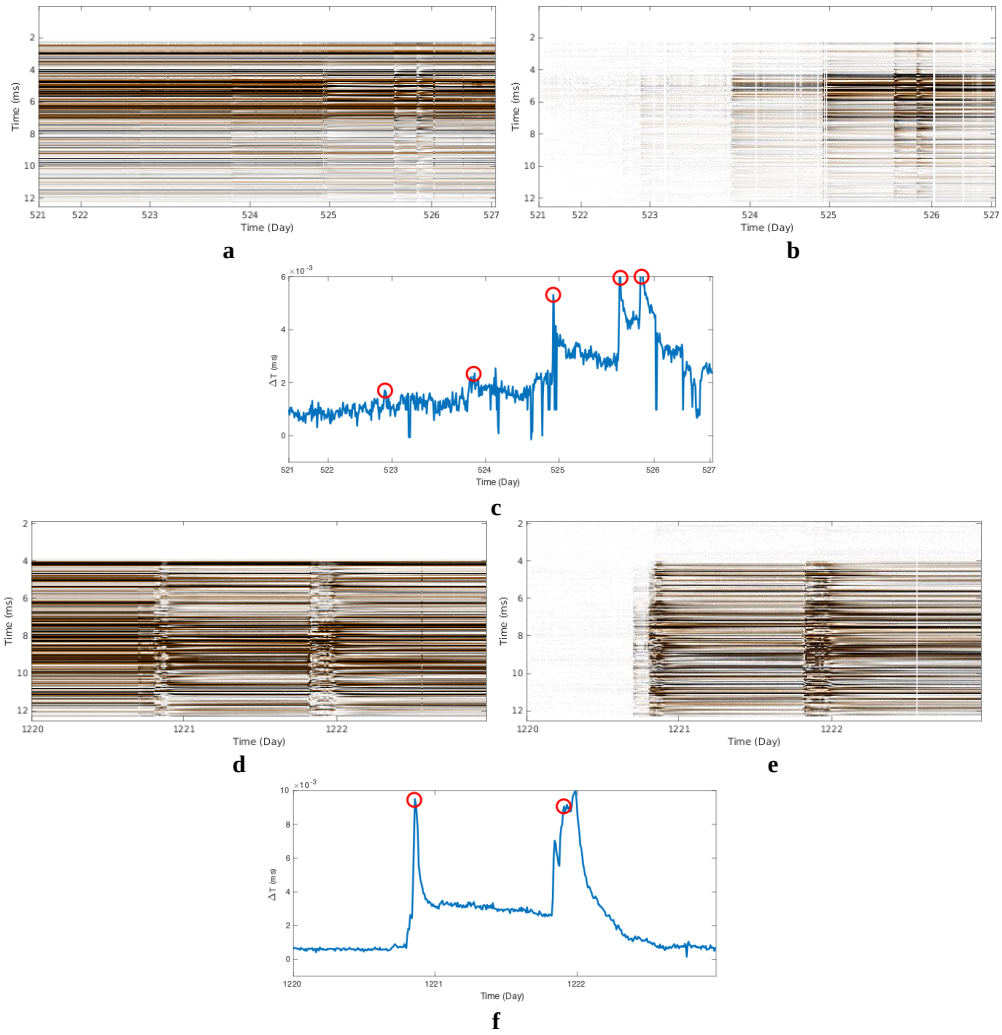

Figure 2: Panels (a) and (d): One recorded CASSM dataset recorded in May, 2018 and in December, 2018, respectively; Panels (b) and (e) are the corresponding time-lapse changes of scattering data caused by the hydraulic stimulations; and Panels (e) and (f) show the corresponding time-lapse changes of first-arrival traveltimes obtained using cross correlation of the time-lapse CASSM waveforms.

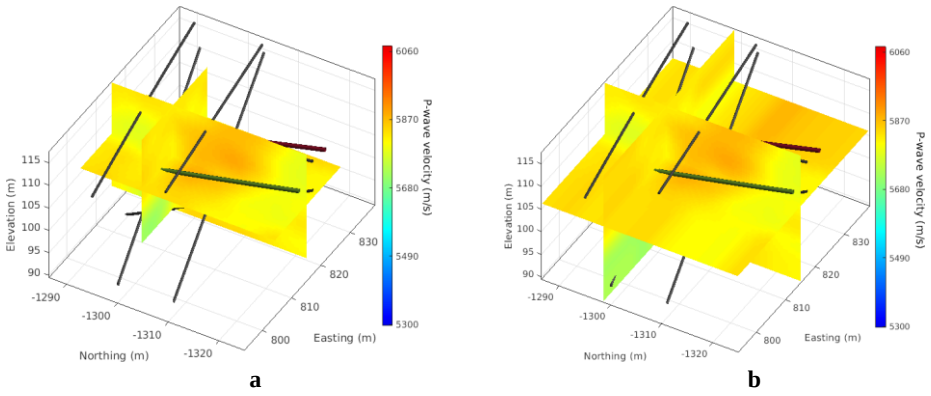

Figure 3: (a) V_{p0} model obtained using 3D anisotropic traveltime tomography and elastic-waveform inversion of the campaign cross-borehole seismic data within the CASSM data acquisition region (Gao et al., 2020), (b) V_{p0} model after extrapolating the model in (a) as the initial model for 3D anisotropic traveltime tomography of the CASSM data.

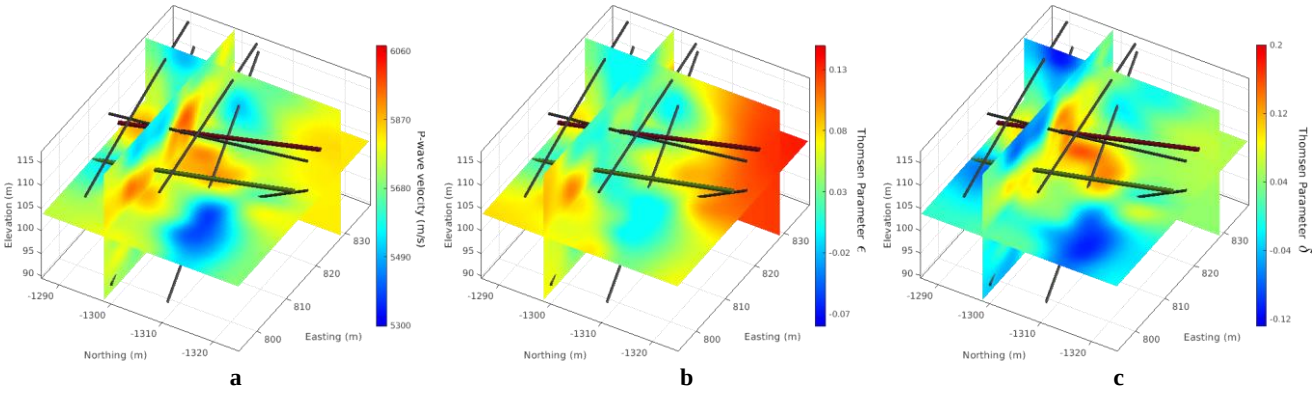

Figure 4: The inverted (a) V_{p0}, Thomsen parameters (b) ϵ and (c) δ models of the CASSM data using 3D anisotropic traveltime tomography of the first-arrival qP-wave events of the baseline CASSM data before hydraulic stimulation in May, 2018.

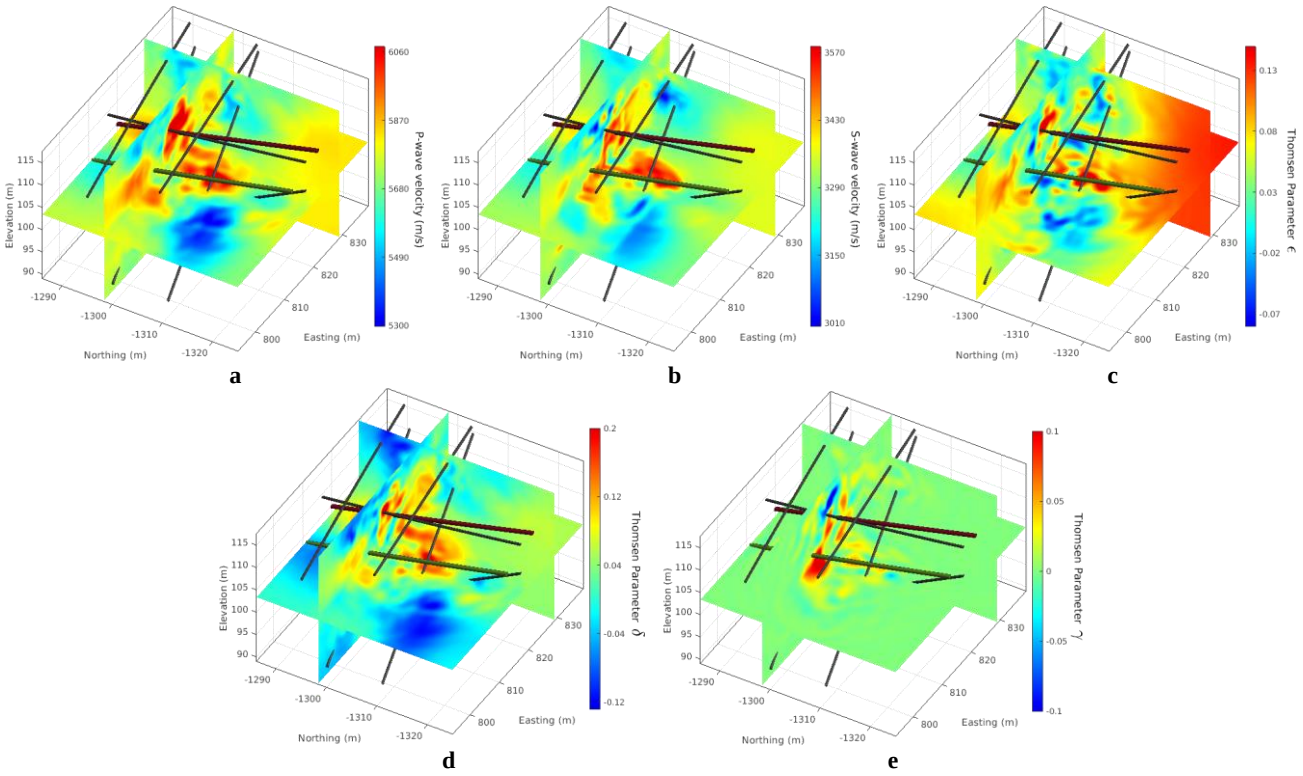

Figure 5: Inversion results of (a) V_{p0}, (b) V_{s0}, Thomsen parameters (c) ϵ, (d) δ, and (e) γ models, obtained using 3D anisotropic elastic-waveform inversion of windowed qP- and the qS-wave direct arrivals of the baseline CASSM data acquired before hydraulic stimulation in May, 2018.

4. RESULTS OF TIME-LAPSE CHANGES

4.1 Traveltime changes caused by hydraulic fracture stimulations

After 3D anisotropic elastic-waveform inversion of the baseline CASSM data, we use waveform cross correction to compute the traveltime changes between the 5 stimulations (red circles in Figure 2c) and the baseline in May, 2018, and between the 2 stimulations (red circles in Figure 2f) and the baseline in December, 2018. We show the traveltime changes for windowed direct qP-wave arrivals and qS-wave arrivals in May, 2018 in Figures 6 and 7, respectively. We also display the traveltime changes for windowed direct qP-wave arrivals and qS-wave arrivals of the CASSM data acquired in December 2018 in Figures 8 and 9, respectively. The traveltime changes show a clear response to the 5 stimulations in May, 2018 and the 2 stimulations in December, 2018. Most of these traveltime changes are traveltime delays, which indicates that seismic velocities decrease after stimulations.

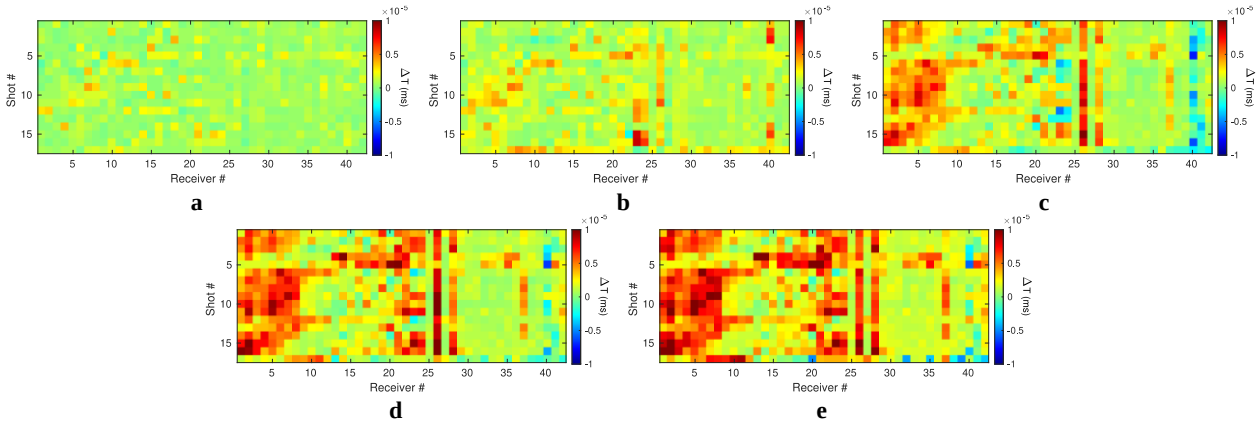

Figure 6: Panels (a) to (e) are the traveltime changes of the windowed direct qP-wave arrivals of the CASSM data acquired after the 1st to 5th hydraulic stimulations in May, 2018. The horizontal number indicates the receiver number with #1~24 for hydrophones and #25~42 for accelerometers. The vertical number denotes the source number.

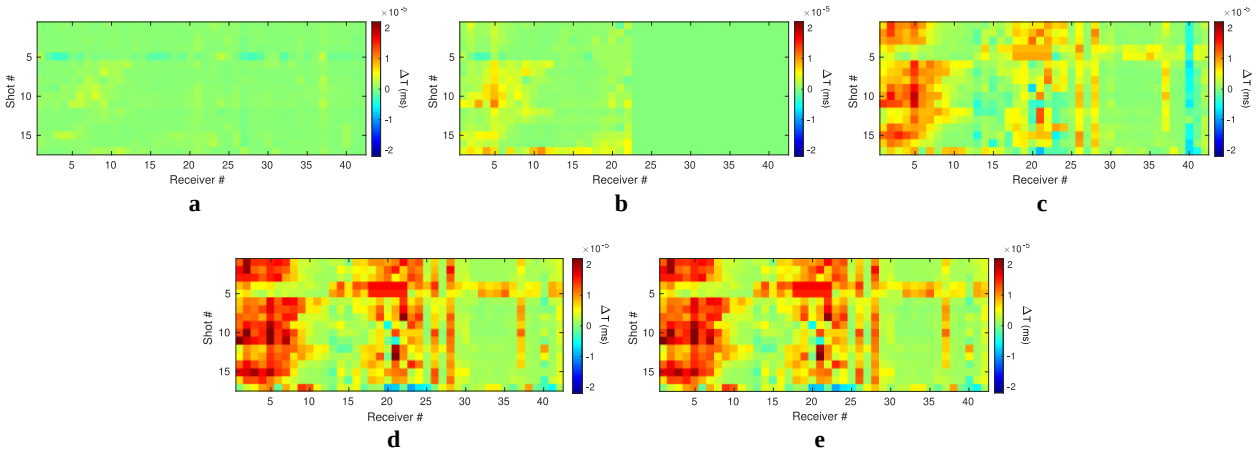

Figure 7: Panels (a) to (e) are the traveltime changes of the windowed direct qS-wave arrivals of the CASSM data acquired after the 1st to 5th hydraulic stimulations in May, 2018.

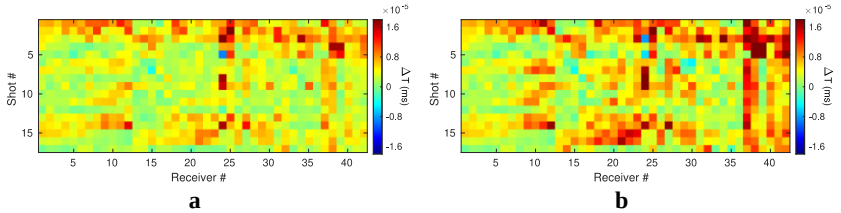

Figure 8: Panels (a) and (b) are the traveltime changes of the windowed direct qP-wave arrivals of the CASSM data acquired after the 1st and 2nd hydraulic stimulations in December, 2018, respectively.

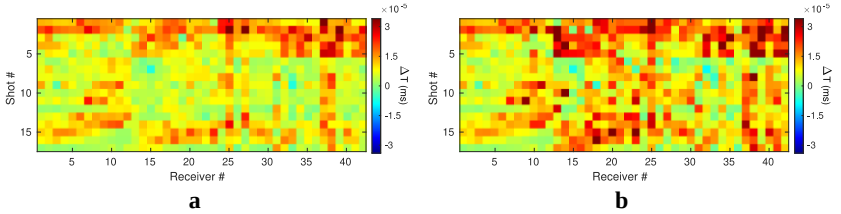

Figure 9: Panels (a) and (b) are the traveltime changes of the windowed direct qS-wave arrivals of the CASSM data acquired after the 1st and 2nd hydraulic stimulations in December, 2018, respectively.

4.2 Temporal-spatial evolution of rock properties caused by hydraulic fracture stimulations

We use the computed traveltime changes of direct qP- and qS-wave arrivals and employ 3D double-difference anisotropic elastic-waveform inversion to jointly update the time-lapse differences of V_{p0}, V_{s0}, and anisotropic parameter models. We display the inverted relative time-lapse changes of V_{p0} and V_{s0} ($\Delta V_{p0}/V_{p0}$ and $\Delta V_{s0}/V_{s0}$) for the 5 stimulations in May, 2018 in Figures 10 and 11, respectively. We depict their contour plots of the relative change ratios with an absolute value of larger than 0.2% in Figures 12 and 13, respectively. The blue regions from Figures 10 and 13 gradually expand in space during the five stimulations, indicating the temporal-spatial evolution of rock properties after hydraulic fracture stimulations in May, 2018. The relative changes of V_{s0} are at the same location as those of V_{p0} except that its scale is smaller.

We show our inversion results of the relative changes of V_{p0} and V_{s0} for the 2 stimulations in December 2018 in Figures 14 and 15, respectively, and their contour plots with an absolute value larger than 0.2% in Figures 16 and 17, respectively. The blue regions from Figures 14 and 17 indicate that the 2 stimulations affect the rock properties similarly. Besides, both the location and the scale of the relative change of V_{s0} are similar to those of V_{p0}. We find that the velocity changes occur around the notch point for hydraulic stimulation (red dots in Figure 18).

The spatial patterns of the relative changes of Thomsen parameters are similar to those of V_{p0} and V_{s0}.

For comparison, we superimpose the microseismic event locations (indicated by the black dots) onto the relative change of V_{p0} for the 5th stimulation in May, 2018 as shown in Figure 18a and 18b, and for the 2nd stimulation in December, 2018 as depicted in Figure 18c and 18d. We find that, in general, the spatial region of the relative V_{p0} change in December 2018 matches well with the region where the microseismic events are located, while the spatial region of the relative V_{p0} change for in May, 2018 locates slightly to the southeast of the region where the microseismic events are located. Note that there may exist some regions with small dry cracks where microseismic events could occur but may not cause measurable changes in elastic parameters.

Our inverted time-lapse changes in seismic velocities and anisotropic parameters result from combined effects of created fractures, fracture opening, injected water, and rock temperature changes (Doetsch el al., 2020; Schopper el al., 2020). Therefore, the region with changes in these elastic parameters indicates the volume of rock alternation caused by hydraulic stimulation.

5. CONCLUSIONS

We have obtained the temporal-spatial evolution of seismic velocities and anisotropic parameters within the hydraulic stimulation region at the first EGS Collab testbed, using 3D anisotropic first-arrival traveltime tomography and 3D anisotropic elastic-waveform inversion of the time-lapse CASSM data acquired before and after each hydraulic fracture stimulation in May, 2018 and in December, 2018. We find that the 5 stimulations in May 2018 gradually expand the spatial regions of changes of rock properties, and the 2 stimulations in December 2018 affect the rock similarly in space. The created fractures, opening of existing fractures, injected water, and the water temperature differences from the host rock, could all caused changes in elastic parameters. Therefore, accurate inversion of time-lapse CASSM data could reliably monitor alternation of the host rock during fracture stimulation in enhanced geothermal systems, including fracture creation and opening and wave movement.

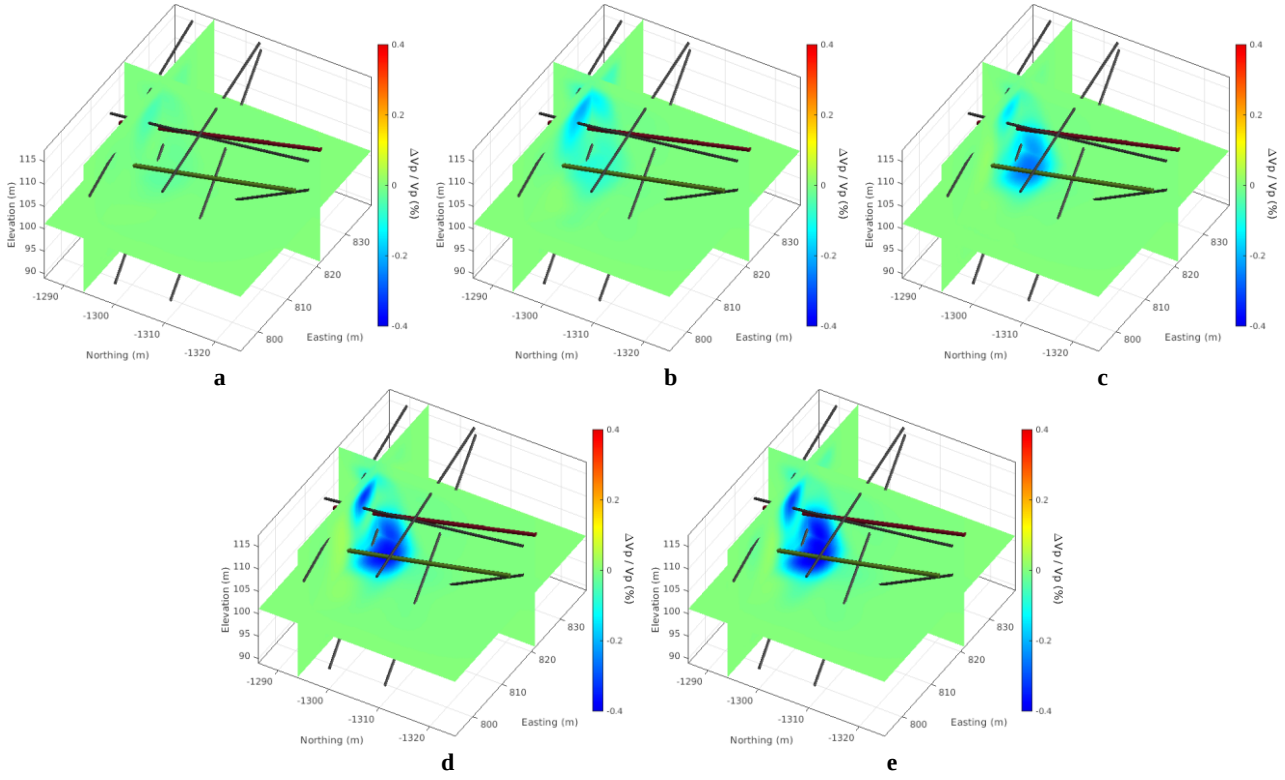

Figure 10: Relative V_{p0} changes obtained using 3D double-difference anisotropic elastic-waveform inversion and the traveltime change of (a) 1st, (b) 2nd, (c) 3rd, (d) 4th, and (e) 5th stimulation in May, 2018 as shown in Figure 6.

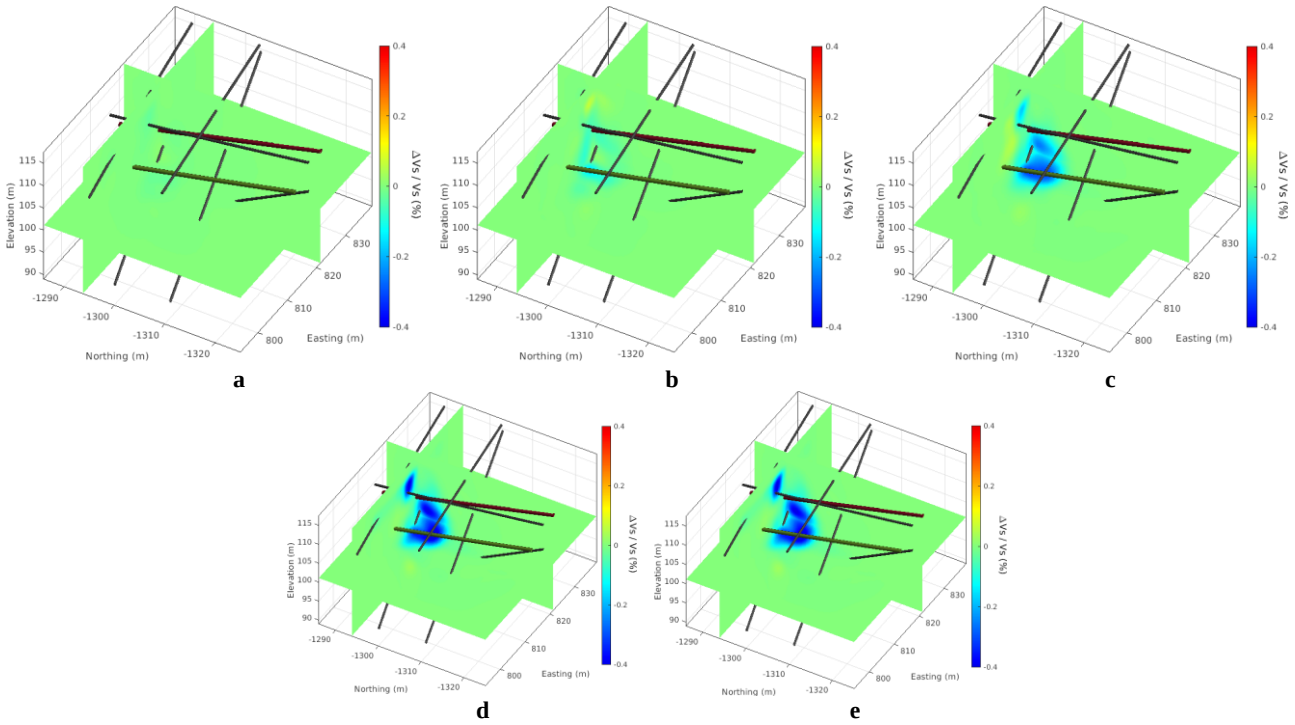

Figure 11: Relative V_{s0} changes obtained using 3D double-difference anisotropic elastic-waveform inversion and the traveltime change of (a) 1st, (b) 2nd, (c) 3rd, (d) 4th, and (e) 5th stimulation in May, 2018 as shown in Figure 7.

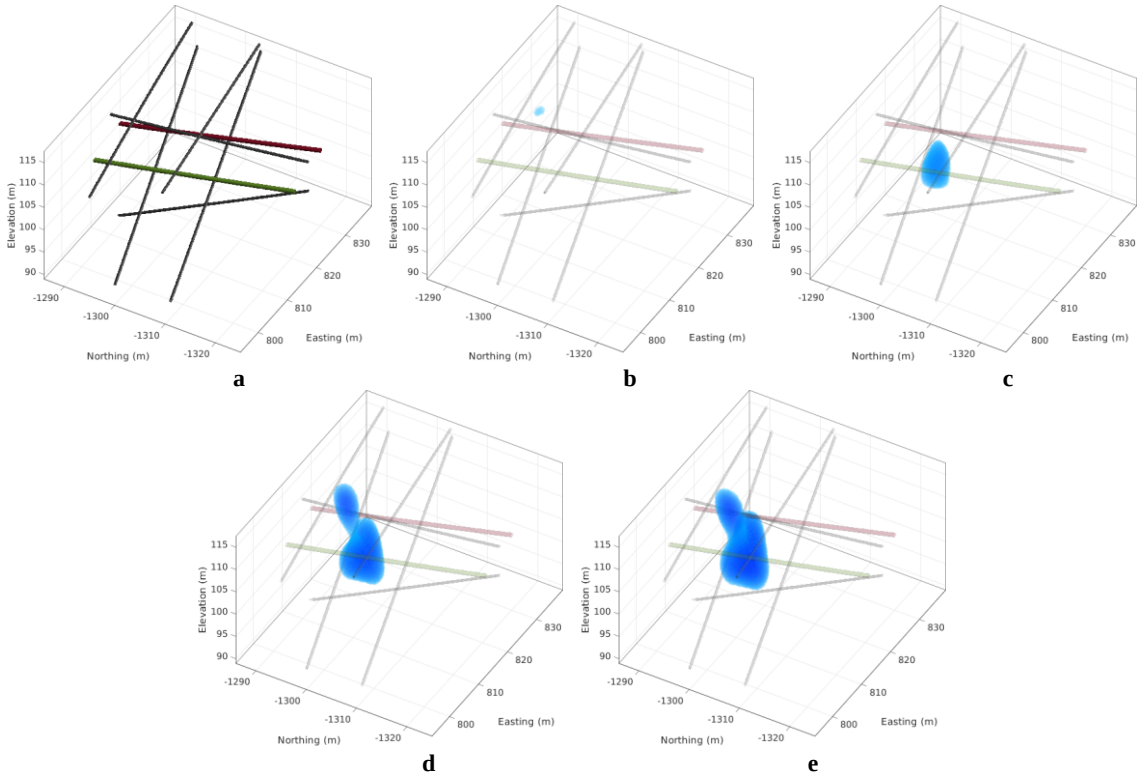

Figure 12: Contour plot of $\Delta V_{p0}/V_{p0}$ with an absolute value of larger than 0.2% for (a) 1st, (b) 2nd, (c) 3rd, (d) 4th, and (e) 5th stimulation in May, 2018, corresponding to Figure 10a to 10e, respectively.

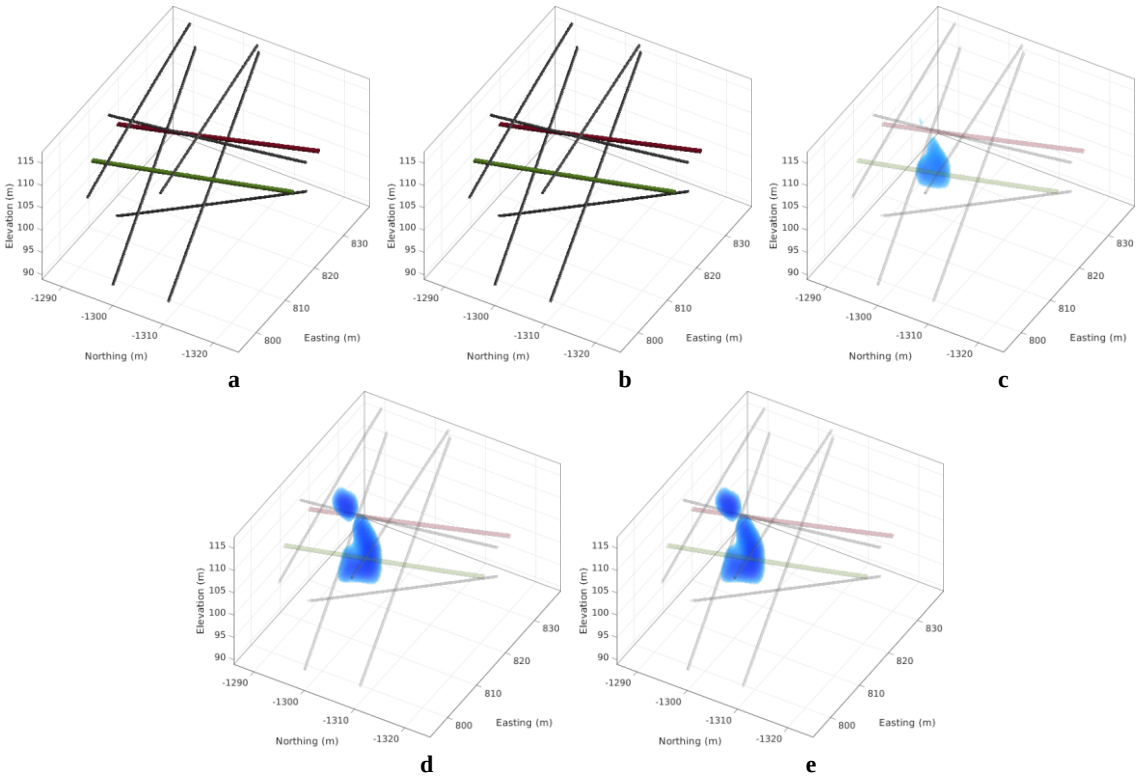

Figure 13: Contour plot of $\Delta V_{s0}/V_{s0}$ with an absolute value of larger than 0.2% for (a) 1st, (b) 2nd, (c) 3rd, (d) 4th, and (e) 5th stimulation in May, 2018, corresponding to Figure 11a to 11e, respectively.

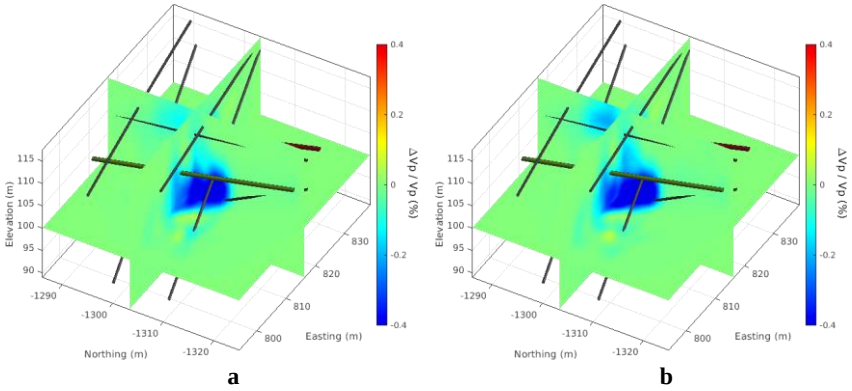

Figure 14: Relative V_{p0} changes obtained using 3D anisotropic elastic-waveform inversion and the traveltime change of (a) 1st and (b) 2nd stimulation in December, 2018 as shown in Figure 8.

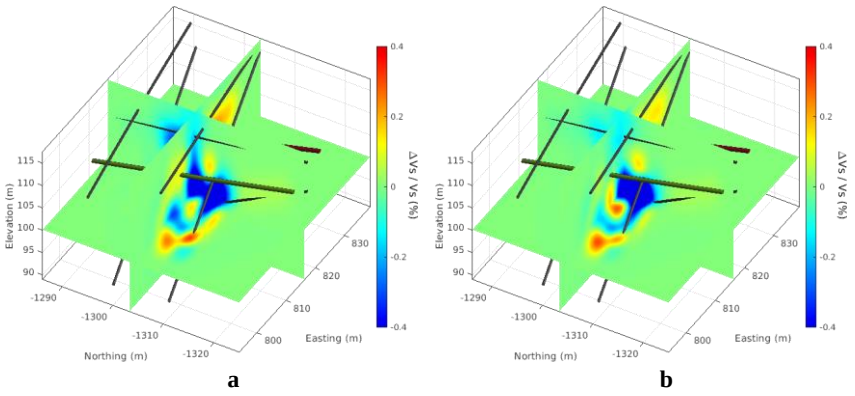

Figure 15: Relative V_{s0} changes obtained using 3D anisotropic elastic-waveform inversion and the traveltime change of (a) 1st and (b) 2nd stimulation in Dcember, 2018 as shown in Figure 9.

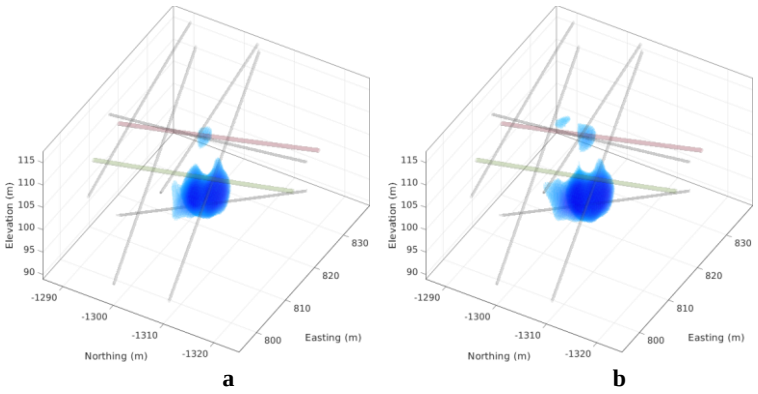

Figure 16: Contour plot of $\Delta V_{p0}/V_{p0}$ with an absolute value of larger than 0.2% for (a) 1st and (b) 2nd stimulation in December, 2018, corresponding to Figure 14a and 14b, respectively.

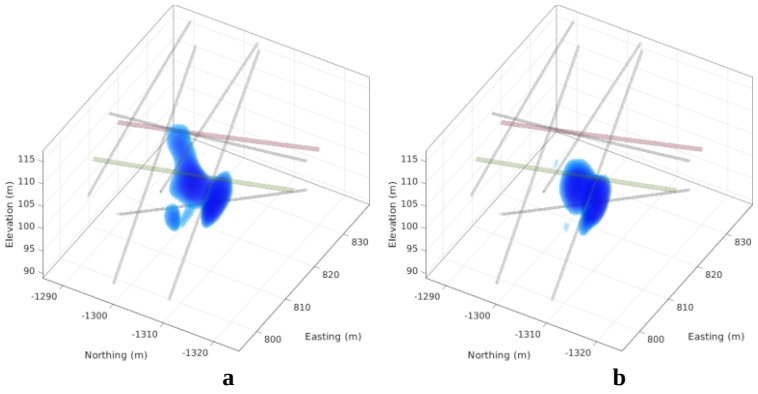

Figure 17: Contour plot of $\Delta V_{s0}/V_{s0}$ with an absolute value of larger than 0.2% for (a) 1st and (b) 2nd stimulation in December, 2018, corresponding to Figure 15a and 15b, respectively.

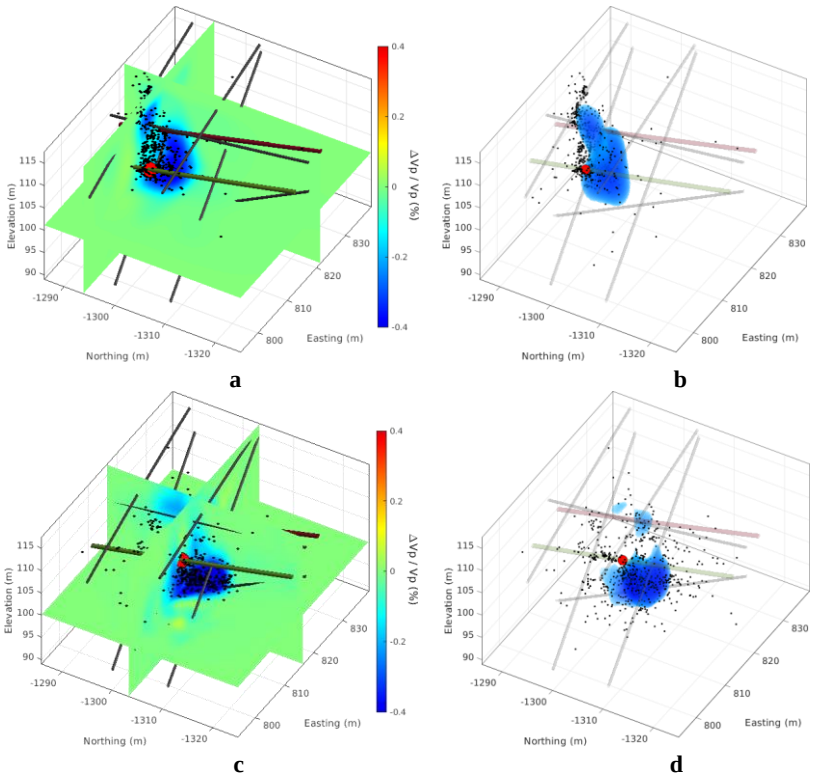

Figure 18: Panels (a) and (b) are relative V_{p0} changes for the 5th stimulation in May, 2018, and Panels (c) and (d) relative V_{p0} changes for 2nd stimulation in December, 2018, superimposed by the microseismic events indicated by the black dots.

ACKNOWLEDGMENTS

This material was based upon work supported by the U.S. Department of Energy (DOE), Office of Energy Efficiency and Renewable Energy (EERE), Office of Technology Development, Geothermal Technologies Office, under Contract No. 89233218CNA000001 to Los Alamos National Laboratory (LANL). LANL is operated by Triad National Security, LLC, for the National Nuclear Security Administration (NNSA) of U.S. DOE. This research used resources provided by the LANL Institutional Computing Program, which is supported by the U.S. DOE NNSA under Contract No. 89233218CNA000001. The United States Government retains, and the publisher, by accepting the article for publication, acknowledges that the United States Government retains a non-exclusive, paid-up, irrevocable, world-wide license to publish or reproduce the published form of this manuscript, or allow others to do so, for United States Government purposes. The research supporting this work took place in whole or in part at the Sanford Underground Research Facility in Lead, South Dakota. The assistance of the Sanford Underground Research Facility and its personnel in providing physical access and general logistical and technical support is acknowledged.

REFERENCES

Berryman, J. G.: Exact Seismic Velocities for VTI and HTI Media and Extended Thomsen Formulas for Stronger Anisotropies (2008).

Chi, B., Huang, L., Gao, K., Ajo-Franklin, J., Kneafsey, T.J., and EGS Collab Team: High-Resolution Imaging of Created Fractures in EGS Collab Experiments Using CASSM Data, *Geothermal Resources Council Transactions*, Geothermal Resources Council Annual Meeting, Palm Springs, CA (2019).

Chi, B., Huang, L., Gao, K., Ajo-Franklin, J., Kneafsey, T.J., and EGS Collab Team: Anisotropic Imaging of Created Fractures in EGS Collab Experiments Using CASSM Data, *Proceedings*, 45th Workshop on Geothermal Reservoir Engineering, Stanford University, Stanford, CA (2020).

Doetsch, J., Gischig, V.S., Villiger, L., Krietsch, H., Nejati, M., Amann, F., Jalali, M., Madonna, C., Maurer, H., Wiemer, S. and Driesner, T.: Subsurface Fluid Pressure and Rock Deformation Monitoring using Seismic Velocity Observations, *Geophysical Research Letters*, **45(19)**, 10-389 (2018).

Gao., K., Huang, L., Knox, H., Schwering, P., Hoots, C., Blankenship, D., Ajo-Franklin, J., Kneafsey, T.J., and EGS Collab Team: Anisotropic Traveltime Tomography of Campaign Cross-Borehole Seismic Data from the First EGS Collab Testbed, *Geothermal Resources Council Transactions*, Geothermal Resources Council Annual Meeting, Palm Springs, CA (2019).

Gao., K., Huang, L., Knox, H., Schwering, P., Hoots, C., Blankenship, D., Ajo-Franklin, J., Kneafsey, T.J., and EGS Collab Team: Anisotropic Elastic Properties of the First EGS Collab Testbed Revealed from the Campaign Cross-Borehole Seismic Data, *Proceedings*, 45th Workshop on Geothermal Reservoir Engineering, Stanford University, Stanford, CA (2020).

Johnson, T., C. Strickland, H. Knox, J. Thomle, V. Vermuel, C. Ulrich, T. Kneafsey, D. Blankenship, and EGS Collab Team: EGS Collab Project Electrical Resistivity Tomography Characterization and Monitoring Status, *Proceedings*, 44th Workshop on Geothermal Reservoir Engineering, Stanford University, Stanford, California, (2019).

Kneafsey, T.J., D. Blankenship, P.F. Dobson, J.P. Morris, M.D. White, P. Fu, P.C. Schwering, J.B. Ajo-Franklin, L. Huang, M. Schoenball, T.C. Johnson, H.A. Knox, G. Neupane, J. Weers, R. Horne, Y. Zhang, W. Roggenthen, T. Doe, E. Mattson, C. Valladao, and the EGS Collab team: The EGS Collab Project: Learnings from Experiment 1, *Proceedings*, 45th Workshop on Geothermal Reservoir Engineering Stanford University, Stanford, CA (2020).

Kneafsey, T.J., D. Blankenship, P.F. Dobson, M.D. White, J.P. Morris, P. Fu, P.C. Schwering, J.B. Ajo-Franklin, L. Huang, H.A. Knox, G. Neupane, J. Weers, R. Horne, W. Roggenthen, T. Doe, E. Mattson, and the EGS Collab team: Fracture Stimulation and Chilled-water Circulation Though Deep Crystalline Rock: Characterization, Modeling, Monitoring, and Heat-transfer Assessment, *Proceedings*, 46th Workshop on Geothermal Reservoir Engineering Stanford University, Stanford, CA (2021).

Luo, Y. and Schuster, G. T.: Wave-equation Traveltime Inversion, *Geophysics*, **56(5)**, (1991), 645-653.

Pan, W., Huang, L., Gao, K., Ajo-Franklin, J., Kneafsey, T.J., and EGS Collab Team: Anisotropic Elastic-Waveform Inversion and Least-Squares Reverse-Time Migration of CASSM Data for Experiment I of the EGS Collab Project, *Proceedings*, 44th Workshop on Geothermal Reservoir Engineering, Stanford University, Stanford, CA (2019).

Schopper, F., Doetsch, J., Villiger, L., Krietsch, H., Gischig, V.S., Jalali, M., Amann, F., Dutler, N. and Maurer, H.: On the Variability of Pressure Propagation During Hydraulic Stimulation Based on Seismic Velocity Observations, *Journal of Geophysical Research: Solid Earth*, **125(2)**, p.e2019JB018801 (2020).

Tsvankin, I., P-wave Signatures and Notation for Transversely Isotropic Media: An Overview, *Geophysics*, **61**, (1996), 467–483.

Zhang, Z. and Huang, L.: Double-Difference Elastic-Waveform Inversion with Prior Information for Time-Lapse Monitoring, *Geophysics*, **78(6)**, (2013), R259-R273.